arXiv:1012.3304v1 [cond-mat.mes-hall] 15 Dec 2010

Spin-Strain Phase Diagram of Defective Graphene

E. J. G. Santos, D. Sánchez-Portal, and A. Ayuela
Centro de Física de Materiales CFM-MPC, Centro Mixto CSIC-UPV/EHU,
Paseo Manuel de Lardizabal 5, 20080 San Sebastián, Spain and
Donostia International Physics Center (DIPC), Paseo Manuel de Lardizabal 4, 20018 San Sebastián, Spain

S. Riikonen
Laboratory of Physical Chemistry, Department of Chemistry,
University of Helsinki P.O. Box 55, FI-00014, Finland

Using calculations on defective graphene from first principles, we herein consider the dependence of the properties of the monovacancy of graphene under isotropic strain, with a particular focus on spin moments. At zero strain, the vacancy shows a spin moment of 1.5 μ_B that increases to $\sim$2 μ_B when the graphene is in tension. The changes are more dramatic under compression, in that the vacancy becomes non-magnetic when graphene is compressed more than 2%. This transition is linked to changes in the atomic structure that occurs around vacancies, and is associated with the formation of ripples. For compressions slightly greater than 3%, this rippling leads to the formation of a heavily reconstructed vacancy structure that consists of two deformed hexagons and pentagons. Our results suggest that any defect-induced magnetism that occurs in graphene can be controlled by applying a strain, or some other mechanical deformations.

Since its discovery[1], graphene has been shown to possess a number of remarkable electronic and elastic properties [2]. Its electronic properties are mainly associated with the p_z orbitals of carbon, while its elastic properties are associated with the *sp* orbitals. Specifically, a Young's modulus of 1 TPa[3] has recently been measured for graphene, in agreement with the average Young´ s modulus for carbon nanotubes of Y =1.25 TPa [4, 5]. Graphene can sustain elastic deformations as large as 20%, and it is typically under a strain of several percent when deposited on surfaces [6]. This strain could be used to engineer the electronic properties of graphene. Unfortunately, a very high tensile force must be applied to defect-free graphene to modify the electronic structure, because the spectrum of planar graphene remains metallic up to 10% stretching[7–9]. However, there are not many experimental conditions under which layers of graphene remain strictly planar. Due to the soft transversal phonons of 2D graphene, at certain temperatures the layer shrinks and ripples are formed. These ripples are present in free-standing layers of pristine graphene[10, 11] and for layers deposited on substrates. [12, 13]. The rippling of graphene induces midgap states [14] in the electronic structure that disappear when relaxations in the layers are carefully taken into account [15]. The relaxations that accompany the rippling of the layer, and their influence on the electronic structure, are particularly important in layers that are under a high degree of compression. Strong rippling of this kind can also be induced by adsorbates [16] and defects [17] such as that recently discovered for OH impurities [11, 18, 19]. Understanding the interaction between defect-induced deformations and ripples is one of the main challenges now faced in the study of the electronic structure of graphene.

In pristine graphene, the *sp* contributions are situated at low energies, and it is the presence of defects that promotes them closer to the Fermi level. By theoretical calculations, it has been shown that substitutional doping[20–23] and the presence of defects[24, 25] in graphene, and in graphitic materials in general, produce magnetism that is of interest in the potential use of these materials in spintronics. In experiments, the irradiation [26–29] and ion bombardment [30] of carbon-based materials create vacancies which indeed are linked with magnetic signals. The vacancies [24, 31, 32] and edges [33, 34] present in graphene layers have been the focus of detailed theoretical studies. Although there have been both studies of the changes in the electronic structure induced by rippling and studies of defects in graphene, to our knowledge there have been no studies of the magnetism of rippled graphene. Such a study is of particular interest when considered alongside the effect of strain on the structural and electronic properties of graphene.

We herein combine the two perspectives and present a study of defective graphene under strain. We focus on a particular type of defect, namely related to carbon monovacancies, and find that these show a rich diversity of structural and spin phase-behavior as a function of strain. For zero strain, each vacancy has a solution with spin moment of 1.5 μ_B. However, non-magnetic solutions become stable under a moderate compression of less than 2% strain. This transition in magnetic moment may be traced to the modification in the local atomic structure of the defect as ripples develop in the layer. In calculations for compressions greater than 3%, the vacancy structure departs from its usual geometry under rippling, and this reconstruction ends with the formation of a different defect structure that has a central atom with strong sp^3 hybridization. All these structural changes are linked with the appearance of ripples as the layer is compressed, similar to those observed in recent experiments [35–37]. We herein explore the relationship between the appearance of rippling patterns, the presence of vacancies, and changes in the electronic and magnetic properties of graphene.

We perform density functional calculations [46] from first principles using the SIESTA code [47]. We use the generalized gradient approximation [48], norm-conserving pseudopotentials [49] and a basis set of numerical atomic orbitals [47]. The integration over the Brillouin zone uses a well-converged Monkhorst-Pack k-sampling [50] that is equivalent to 70×70 points for the graphene unit cell. The structural optimizations use the conjugate gradient algorithm, which causes the forces to converge until they are lower than 0.05 eV/Å.

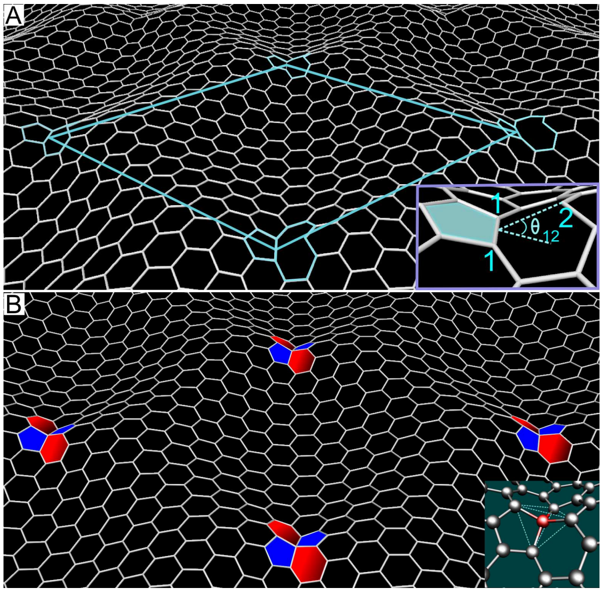

FIG. 1. (A) Graphene with vacancies under an isotropic compression of 1.2%. As an example we use the 10×10 unit cell (highlighted). The inset shows the geometry of the vacancies and the atomic labels. The local bending at the vacancies is described by the angle θ_{12} between the pentagon and the plane defined by three C atoms around the vacancy, i.e. two equivalent atoms labeled 1 and a third atom labeled 2. Note the rippling of graphene sheets with vacancies at the saddle points. (B) A different vacancy structure for a compression slightly under 3%. It has two distorted hexagons and pentagons, while the central C atom shows strong sp^3 hybridization.

Structure versus strain. While under tension the layer remains perfectly flat, and small compressions produce the spontaneous rippling of graphene with a characteristic deformation around the vacancy. 1 illustrates the rippled geometry after relaxing one of our models for a free-standing defective graphene layer under an isotropic compression of 1.2%. At zero strain, the monovacancy tends to undergo a Jahn-Teller–like distortion that lowers its energy by ∼200 meV: atoms of type 1 (see the inset of 1) reconstruct to form a pentagon with the neighboring atoms, while atom 2 is left with the dangling bond responsible for the spin polarization. Although we herein consider a non-planar structure under strain, our findings at low compressions are similar to results previously obtained for flat graphene [38, 39]. However, atom 2 in our rippled structure is progressively lifted from the graphene surface by as much as ∼1.0 Å for strains slightly below 3%, just before the occurrence of a strong vacancy reconstruction. The data of 1B reveal a particularly striking result. In contrast to 2D vacancy, for which previous authors invariably described a 'pentagon-goggles' structure, our own calculations show that the vacancy is strongly reconstructed under rippling. For compressive strains greater than 3%, a different defect structure is produced altogether, consisting of two heavily distorted hexagons and pentagons and resembling the transition states of a planar vacancy movement. We shall now focus on the description of this region of transition for compression of up to 2.8%.

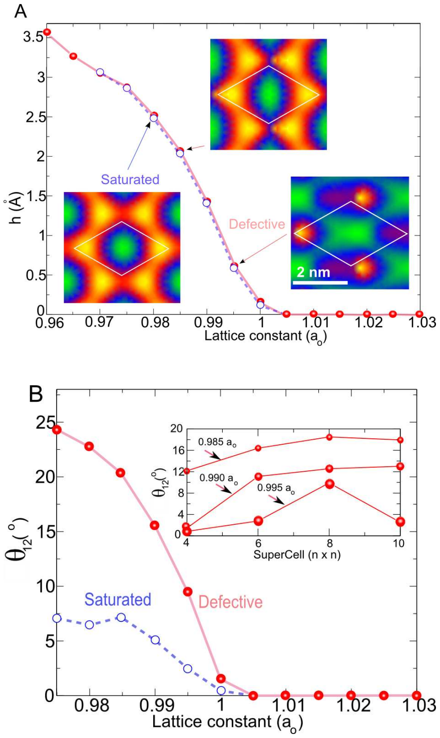

FIG. 2. (A) Maximum amplitude h(Å) of rippling for 10×10 graphene supercells versus strain in units of the equilibrium lattice constant a_o. The filled circles denote defective graphene, while the empty circles denote the pristine layer that has been recovered by adding a carbon atom to the vacancy. The insets show the corrugation patterns: the bright/yellow (dark/green) areas indicate the higher (lower) regions. (B) Bending angle θ_{12} (see definition in 1) as a function of strain. The inset shows the behavior of the bending angles with size of supercell for different values of strain. The local induced deformation clearly depends on the presence of vacancies and on the size of the supercell.

2A shows the maximum amplitude of the rippling h as a function of strain for defective graphene (shown by the solid symbols). We removed the defects from each rippled structure by adding carbon atoms to the vacancy sites and relaxing the structure. We obtained rippled pristine graphene with maximum amplitudes as shown in 2 (open symbols). The amplitudes and the topographic patterns (insets in 2A) show little difference between pristine or defective graphene, particularly for compressive strains greater than ∼1%. It seems that even for large supercells, the main determinant to get ripples is the applied strain. However, the structural patterns that occurs in defective graphene define a preferential direction and break the up-down symmetry that exits perpendicular to the layer. It is this preferential direction and the breaks in the symmetry that are explained by the reconstructed vacancies, which break the hexagonal symmetry of graphene with their goggles-pentagon structure. Vacancies thus play a key role in determining the shape and symmetry of the global deformation patterns of graphene.

We simultaneously characterize the local curvature at the vacancies and the height of atom 2 above the local tangent-plane in terms of the bending angle θ_{12}, as defined in 1. In 2B, we plot the bending angle for both defective and pristine graphene. Under moderate compression (1-2%), the local bending angle for defective graphene is about three times greater than that of pristine graphene and the graphene rippling is clearly made easier by the presence of the vacancies. The dependence of θ_{12} on the size of the supercell, as shown in the inset of 2B, further demonstrates the coupling between the local geometry of the defect and the global deformation, in that for 4×4 supercell, a strain larger than 1.0% is required to obtain an increase in θ_{12} and to allow the corrugation of the layer to begin. However, for larger supercells, much smaller strains cause appreciable deformations around the vacancies.

Energetics. The range of applied strain used here (a few percent) is comparable to that used in experiments in which an appreciable corrugation of graphene was reported for supported layers [36, 40, 41], chemically functionalized graphene [16] , or defective layers [17]. As a result of the imposed periodicity and the finite-sizes used in our calculations, long-wavelength deformations appear primarily to be related to the strain, i.e. vacancies do not create significant corrugation in the relaxed geometry at the equilibrium lattice constant. However, we observe that for the range of strain considered here, the system is compressed and thereby assumes a rippled configuration at an energy between two and three times lower for defective graphene than for the pristine layer. For a 10x10 supercell, the energy required to create ripples for a compression of 3% is reduced to almost half its value in the presence of vacancies, as seen in 3A. This difference in energy is consistent with the proposed role of vacancies as a source of ripples in recent experiments [17].

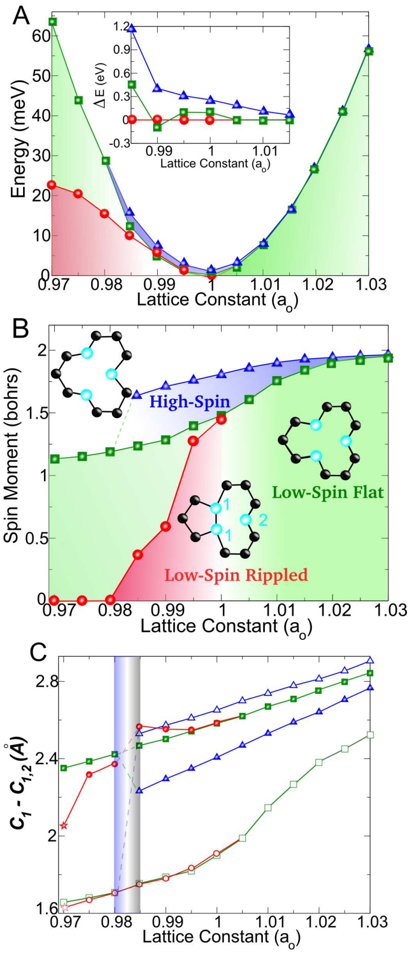

FIG. 3. Variation in total energy per atom (A), spin moment (B), and bond length (C) versus strain for three different configurations of vacancy in the 10×10 supercell: high-spin flat (triangles), low-spin flat (squares) and low-spin rippled (circles). The inset in panel (a) details the change in total energy with respect to the low-spin solutions at about zero strain. The filled and empty symbols in panel (C) represent the 1-2 and 1-1 distances, respectively (see the inset of 1 for atomic labels). The marks given by stars refer to the average distances as the geometry departs from the usual vacancy to the structure in 1B. Note that the magnetism disappears at a strain of ∼2% when allowing if out-of-plane deformations are allowed.

Magnetism versus strain: several spin solutions. In the foregoing part we commented on the fact that isotropic strain can be used to tune the vacancy structure and the curvature of the layer at the site of the defect. We now focus on the influence of these structural changes on the magnetic and electronic properties of the vacancies. We first consider the case of zero strain, i.e. at the equilibrium lattice constant. The usual reconstruction [38, 39] is accompanied by a decrease in the 1-1 distance in 1 and an increase in the 1-2 distances. The two dangling bonds in the type 1 atoms are thus saturated while atom 2 remains uncoordinated. It is the polarization of the corresponding dangling bond that is the main reason behind the appearance of a spin moment of $\sim 1.5\mu_B$ associated with the carbon monovacancy. However, we were able to stabilize another reconstruction characterized by a different structural distortion, in which the 1-2 distance decreases, while the 1-1 distance increases [see the local structures and distances in 3B,C]. This structure has a larger spin moment of $\sim 1.82\mu_B$. We refer to this latter structure as the high-spin (HS) configuration, and to the former as the low-spin (LS) configuration. At zero strain the LS structure is more stable than the HS by around 250 meV.

The behavior of these two structures as a function of strain is summarized in 3. When applying tension to the layer, both the HS and LS structures remain flat and almost become degenerate. In both cases the spin moments show a slight increase. Conversely, when the layer is compressed, the HS structure becomes unstable. Indeed, it is only possible to stabilize the HS configuration under compression provided that the layer is constrained to remain flat. Even for flat graphene, the energy difference between the HS and LS states increases significantly with compression, and for strains greater than 1.5% the HS configuration spontaneously transforms into LS-flat (i.e. low-spin constrained to be flat). In both structures, the spin moments decrease as the layer is compressed. The change is greater for the LS-flat configuration, which varies from 1.98 μ_B for a +3% deformation to 1.15 μ_B at −3%. A more dramatic reduction in the spin moment is seen if ripples are allowed to form in the graphene layer. 3B shows that the spin moment of the LS-rippled (i.e. low-spin free to ripple) vacancy decreases sharply when the compressions exceeds 0.5%. In fact, the ground state of the monovacancy becomes non-magnetic for compressive strains in the range of 1.5-2%.

The changes in the spin moments of vacancies may be understood by analyzing their electronic structure. When carbon atom 2 is restricted to remain in the plane, the spin moment is mainly associated with the sp^2 dangling bond, and the contribution from the p_z states is smaller. The strain-induced deformation of the vacancy and subsequent out-of-plane displacement of atom 2 gives rise to the hybridization between the out-of-plane p_z states and the in-plane sp^2 states. For flat graphene the spin-polarized impurity level associated with the vacancy therefore has a strong sp^2 character and remains essentially decoupled from the delocalized electronic levels of graphene due to their different symmetries. For the rippled layer, these two types of electronic states are strongly hybridized. This hybridization results in the delocalization of the defect levels which eliminate the magnetism and explains why the LS-rippled configuration has a lower spin moment. Expressed in three dimensions, the rippling is believed to transform the hybridization of the C vacancy atoms in sp^3, thereby removing the cause of local magnetism, as seen at the higher compression of the case of 1B.

Rippling of the graphene layer occurs in a range of cases. One such case is where graphene is deposited on substrates, in which there is a significant mismatch in between lattice parameters. For example, ripples have been previously observed for graphene deposited on Ru(0001) [36], as well as on other metallic substrates. Strain can also be applied and controlled by placing exfoliated graphene on flexible substrates, as reported recently [42, 43]. Under such conditions, it may be possible to create defects in regions of different curvature using a focused electron beam, by applying a technique similar to that recently demonstrated by Rodriguez-Manzo and Banhart [44]. The existence and spatial distribution of the spin moment associated with the vacancies, and its variations with deformation, could then in principle be monitored using a spin-polarized scanning tunneling microscope. [30, 45]

In summary, we have shown that the magnetic and structural properties of carbon vacancies depend strongly on the local curvature induced by defects. Together with the global rippling pattern, this curvature can be controlled by the application of a strain. By compressing graphene by up to 2%, we can adjust the spin moment of the vacancy to between 0 and 1.5 μ_B. At our high-compression limit, the rippling allows the defect C atoms to be arranged in a geometry that is different from the vacancy as generally observed. Such strains may be achieved experimentally [42, 43] and are comparable with those found when graphene is deposited on a range of different substrates. In fact, our results suggest that the magnetism that is induced in graphene by the presence of defects can be controlled using isotropic strain and other mechanical deformations.

Acknowledgment. We acknowledge the support of the Basque Departamento de Educación and the UPV/EHU (Grant No. IT-366-07), the Spanish Ministerio de Innovación, Ciencia y Tecnología (Grant No. FIS2007-66711-C02-02), and the ETORTEK research program funded by the Basque Departamento de Industria and the Diputacíon Foral de Guipuzcoa.

---

[1] A. K. Geim and K. S. Novoselov, Nat. Mater. **6**, 183 (2007).

[2] K. S. Novoselov and other, Proc. Natl. Acad. Sci. U.S.A. **102**, 10451 (2005).

[3] C. Lee *et al.*, Science **321**, 385 (2008).

[4] A. Krishnan *et al.*, Phys. Rev. B **58**, 14013 (1998).

[5] G. Overney, W. Zhong, and D. Tomanek, Z. Phys. D **27**, 93 (1993).

[6] M. Huang *et al.*, Proc. Natl. Acad. Sci. U.S.A. **106**, 7304 (2009).

[7] G. Gui, J. Li, and J. Zhong, Phys. Rev. B **78**, 075435 (2008).

[8] V. M. Pereira, A. H. C. Neto, and N. M. R. Peres, Phys Rev B **80**, 045401 (2009).

[9] G. Cocco, E. Cadelano, and L. Colombo, Phys. Rev. B **81**, 241412R (2010).

[10] A. Fasolino, J. Los, and M. I. Katsnelson, Nat. Mater. **6**, 858. (2007).

[11] D. Boukhalov and M. I. Katsnelson, J. Am. Soc. **130**, 10697 (2008).

[12] E. Stolyarova *et al.*, Proc. Natl. Acad. Sci. U.S.A. **104**, 9209 (2007).
[13] M. Ishigami *et al.*, Nano Lett. **7**, 1643. (2007).
[14] F. Guinea, M. I. Katsnelson, and M. A. H. Vozmediano, Phys. Rev. B **77**, 075422 (2008).
[15] T. O. Wehling *et al.*, Eur. Phys. Lett. **84**, 17003 (2008).
[16] H. C. Schniepp *et al.*, ACS Nano **2**, 2577 (2008).
[17] U. Bangert *et al.*, Phys. Stat. Sol. A **206**, 1117 (2009).
[18] R. C. Thompson-Flagg, M. J. B. Moura, and M. Marder, Eur. Phys. Lett. **85**, 46002. (2009).
[19] C. Gómez-Navarro *et al.*, Nano Lett. **10**, 1144 (2010).
[20] E. J. G. Santos *et al.*, Phys. Rev. B **78**, 195420 (2008).
[21] E. J. G. Santos, D. Sánchez-Portal, and A. Ayuela, Phys. Rev. B **81**, 125433 (2010).
[22] E. J. G. Santos, A. Ayuela, and D. Sánchez-Portal, New J. Phys. **12**, 053012 (2010).
[23] Y. Lee, S. Kim, and D. Tománek, Phys. Rev. Lett. **78**, 2393 (1997).
[24] Y. Ma *et al.*, New J. Phys. **6**, 68 (2004).
[25] P. Lehtinen *et al.*, Phys. Rev. Lett. **91**, 017202 (2003).
[26] P. Esquinazi *et al.*, Phys. Rev. Lett. **91**, 227201 (2003).
[27] H. Ohldag *et al.*, **98**, 187204 (2007).
[28] A. V. Krasheninnikov and F. Banhart, Nat. Mater. **6**, 723 (2007).
[29] C. Gomez-Navarro *et al.*, Nature Materials **4**, 534 (2005).
[30] M. M. Ugeda *et al.*, Phys. Rev. Lett. **104**, 096804 (2010).
[31] V. M. Pereira *et al.*, Phys. Rev. Lett. **96**, 036801 (2006).
[32] O. V. Yazyev, Phys. Rev. Lett. **101**, 037203 (1998).
[33] M. Fujita *et al.*, Phys. Soc. Jap. **65**, 1920. (1996).
[34] T. Enoki, Y. Kobayashi, and K. I. Fukui, Int. Rev. Phys. Chem. **26**, 609 (2007).
[35] J. C. Meyer *et al.*, Nature **446**, 60. (2007).
[36] A. L. V. de Parga *et al.*, Phys. Rev. Lett. **100**, 056807 (2008).
[37] V. Geringer *et al.*, Phys. Rev. Lett. **102**, 076102 (2009).
[38] H. Amara1 *et al.*, .
[39] A. A. El-Barbary *et al.*, Phys. Rev. B **68**, 144107 (2003).
[40] J. Röhrl *et al.*, Appl. Phys. Lett. **92**, 201918 (2008).
[41] G. M. Rutter *et al.*, Phys. Rev. B **76**, 235416 (2007).
[42] T. M. G. Mohiuddin *et al.*, Phys. Rev. B **79**, 205433 (2009).
[43] K. S. Kim *et al.*, Nature **457**, 706 (2009).
[44] J. A. Rodriguez-Manzo and F. Banhart, Nano Lett. **9**, 2285 (2009).
[45] R. Wiesendanger, Rev. Mod. Phys. **81**, 1495 (2009).
[46] W. Kohn and L. J. Sham, Phys. Rev. **140**, A1133 (1965).
[47] J. M. Soler *et al.*, J. Phys.: Conden. Matter **14**, 2745 (2002).
[48] J. P. Perdew, K. Burke, and M. Ernzerhof, Phys. Rev. Lett. **77**, 3865. (1996).
[49] N. Troullier and J. L. Martins, Phys. Rev. B **43**, 1993 (1991).
[50] H. J. Monkhosrt and J. D. Pack, Phys. Rev. B **13**, 5188 (1976).